Biochemistry

Communication

Cite This: Biochemistry 2018, 57, 1572−1576

pubs.acs.org/biochemistry

The Single-Molecule Centroid Localization Algorithm Improves the Accuracy of Fluorescence Binding Assays

Boyang Hua,[†] Yanbo Wang,[†] Seongjin Park,[∥,#] Kyu Young Han,[∥,@] Digvijay Singh,[†] Jin H. Kim,[⊥,∇] Wei Cheng,[⊥] and Taekjip Ha[*,†,‡,§]

[†]Department of Biophysics and Biophysical Chemistry, Johns Hopkins School of Medicine, Baltimore, Maryland 21205, United States

[‡]T. C. Jenkins Department of Biophysics, Johns Hopkins University, Baltimore, Maryland 21218, United States

[§]Howard Hughes Medical Institute, Baltimore, Maryland 21205, United States

[∥]Department of Physics, University of Illinois at Urbana-Champaign, Urbana, Illinois 61801, United States

[⊥]College of Pharmacy, University of Michigan, Ann Arbor, Michigan 48109, United States

Supporting Information

ABSTRACT: Here, we demonstrate that the use of the single-molecule centroid localization algorithm can improve the accuracy of fluorescence binding assays. Two major artifacts in this type of assay, i.e., nonspecific binding events and optically overlapping receptors, can be detected and corrected during analysis. The effectiveness of our method was confirmed by measuring two weak biomolecular interactions, the interaction between the B1 domain of streptococcal protein G and immunoglobulin G and the interaction between double-stranded DNA and the Cas9−RNA complex with limited sequence matches. This analysis routine requires little modification to common experimental protocols, making it readily applicable to existing data and future experiments.

Biomolecules, such as proteins and nucleic acids, interact with each other inside cells during their various functions. It is often informative to determine the kinetic and equilibrium constants of these interactions. One can perform binding assays to determine these constants.[1] When combined with single-molecule detection capability, binding assays can detect the events of single-biomolecule complex formation and dissociation.[2,3] In a commonly used single-molecule assay format, one biomolecule of interest is immobilized on an imaging surface while its binding partner that is fluorescently labeled is introduced in solution. Figure 1a shows a representative frame from a single-molecule movie obtained from such an experiment (Video S1). Each fluorescent spot, which may represent an individual complex formed by two biomolecules, can be detected by single-molecule spot detection routines, and its fluorescence intensity can be extracted through a Gaussian-weighted summation method. The centermost pixel has the highest weight (1.00) in the total intensity calculation, while each of the surrounding pixels has a lower weight (<1.00). A typical Gaussian kernel is shown in Figure 1b. For the sake of simplicity, we will, in this paper, call the surface-immobilized molecules "receptors" and their binding partners in solution "ligands". When this analysis is performed for every frame in a single-molecule movie, an intensity−time trajectory can be generated for each receptor (Figure 1c). From these trajectories, one can determine the dwell times of ligand-bound (high fluorescence) and unbound (low fluorescence) states.

A common artifact, however, in single-molecule fluorescence binding assays comes from nonspecific binding of ligands to the imaging surface. These nonspecific binding events occur randomly and uniformly on the surface unless passivation defects exist, which preferentially attract ligands. Nonspecific binding events can be partly rejected during analysis by including only those events that co-localize with fluorescently labeled receptors through multicolor labeling and imaging.[4] However, for conventional wide-field microscopy, the diffraction-limited resolution is much larger than the size of a ligand−receptor complex (lateral resolution of ∼260 nm at λ_{em} = 620 nm and objective NA = 1.2). Consequently, diffraction-limited co-localization analysis cannot reject nonspecific binding events that occur closer to a receptor than the resolution; the analyzed intensity−time trajectory of that receptor is therefore "contaminated" by these nonspecific binding events. In some severe cases, intensity−time trajectories obtained around passivation defects could contain mainly nonspecific binding events. Effective surface passivation can alleviate the issue of nonspecific binding [see the comparison between the PEG and dichlorodimethylsilane-Tween 20 (DT20) surfaces (Figure S1)] and is typically required in single-molecule fluorescence binding assays.[5]

In addition to nonspecific binding, insufficient optical resolution can lead to another artifact; i.e., when multiple receptors are located closer together than the resolution, specific binding events at these closely spaced receptors cannot be distinguished. We will define the "minimal detection area" as an area on the imaging surface that has a radius equal to the resolution. Quantitatively, apparent binding rate constant $k_{on,app}$ is given by $k_{on,app} = nk_{on} + A\Psi_{on,ns}$, where n is the number of receptors within a minimal detection area, k_{on} is the specific binding rate constant of a single receptor, A is the size of a minimal detection area, and $\Psi_{on,ns}$ is the flux of nonspecific binding events per unit ligand concentration (thus $\Psi_{on,ns}$ has

Received: December 22, 2017
Revised: February 10, 2018
Published: February 19, 2018

DOI: 10.1021/acs.biochem.7b01293
Biochemistry 2018, 57, 1572−1576

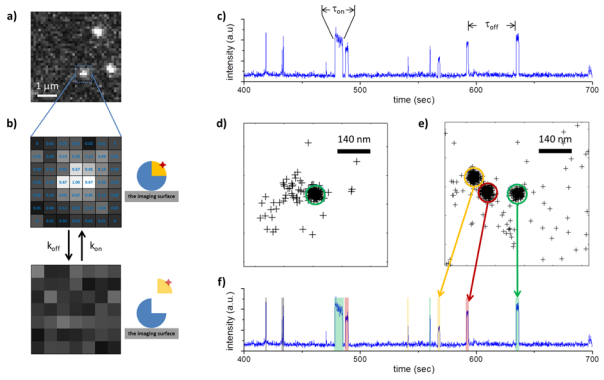

Figure 1. Single-molecule fluorescence binding assays. (a) A representative frame from a single-molecule movie obtained by single-molecule fluorescence binding assays. In this case, the immobilized receptors were immunoglobulin G molecules, and the ligands were B1 domain of streptococcal protein G molecules (labeled with Alexa 594). The ligand concentration used here was 10 nM. (b) A close-up of an individual spot. Its fluorescent intensity can be extracted by using a Gaussian-weighted summation method. When all the 7×7 pixel intensities are summed, each pixel has a different weight based on its distance from the centermost pixel. The weight of each pixel follows a Gaussian kernel $e^{-0.4(\text{pixel distance})^2}$. The spot disappears when the fluorescently labeled ligand dissociates from the receptor. Each pixel shown in panels a and b is 125 nm. (c) An example intensity−time trajectory generated by analyzing and extracting the intensity from each frame in a single-molecule movie. From the intensity−time trajectory, dwell times of the ligand-bound and unbound states can be calculated. (d and e) Using the single-molecule centroid localization algorithm, one can determine the positions of binding events with molecular scale precision. One binding event usually consists of multiple localization events (black marks, Methods). Localization information reveals nonspecific binding events (localization events outside the green circle in panel d) and closely spaced receptors (localization events in different clusters in panel e). (f) On the basis of localization information, one can adjust the intensity−time trajectory shown in panel c to account for measurement artifacts. Specific binding events (colored peaks) were assigned to different receptors, while nonspecific binding ones (gray peaks) were unassigned.

units of μm^{-2} μM^{-1} s^{-1}). The apparent binding rate constant can be falsely high when n is an integer greater than 1 and when the $A\Psi_{on,ns}$ term is non-negligible as compared to k_{on}.

One way to resolve these issues is to reduce the minimal detection area (or volume for three-dimensional detection). This was previously achieved by using zero-mode waveguides or plasmonic nanoantennas.[6,7] However, these methods are relatively complicated to implement and therefore are not readily accessible to most laboratories. Point accumulation for imaging in nanoscale topography (PAINT[8]) and its derivative DNA-PAINT[3] have been used to resolve spatially close receptors. Intermittency in the fluorescence signal required for localization-based super-resolution imaging is linked directly to the kinetic constants of binding and dissociation in PAINT. PAINT therefore has been repurposed to map binding "hot spots" on DNA origamis and to determine the stoichiometry of biological complexes.[9,10] However, these studies largely focused on DNA-based systems.

Here, we propose to use the single-molecule centroid localization algorithm (also used in PAINT) to determine the positions of binding events with molecular scale precision and to enable accurate kinetic measurements of molecular interactions. The stochastic nature of binding and dissociation ensures image sparsity for super-resolution imaging.[8] When imaged at a resolution comparable to the size of ligand−receptor complexes, specific binding events at a single receptor appear within a small cluster (full width at half-maximum of ∼30 nm), where successive binding and dissociation events happen repeatedly (Figure 1d, inside the circle). Random nonspecific binding events occur in a scattered fashion, mainly outside specific clusters (Figure 1d, outside the circle). Closely spaced receptors can also be resolved (Figure 1e). Single-molecule localization information thus allows us to correct the raw intensity−time trajectories to remove most measurement artifacts (Figure 1f). On the basis of this additional level of information from the single-molecule centroid localization algorithm, we have developed a workflow to extract the corrected intensity−time trajectories for single receptors as illustrated in Figure S2.

To test the effectiveness of the proposed method, we measured the kinetic and equilibrium constants of the interaction between the B1 domain of streptococcal protein G (pGB1) and rabbit immunoglobulin G (IgG). Because of its generally high binding affinities for IgG from many species, protein G has been used in a variety of immunoassays for the detection of antibodies. The full-length protein G (pG) is made of three almost identical domains (B1−B3) linked by peptide linkers.[11] Previous studies have shown that pG has a picomolar affinity for IgG.[12] However, for truncated pG with only two or one of the three repeat domains, their affinities are reduced by 1 or 4 orders of magnitude, respectively.[13−17] We chose to measure the interaction between IgG and pG with only one repeat domain (pGB1), for it is known to be difficult to measure low-affinity interactions (K_D in the approximately micromolar range) with single-molecule methods.[18]

We immobilized IgG on a DT20 imaging surface through a biotin−neutravidin linker and added pGB1 that was stoichiometrically labeled with Alexa 594 at a single cysteine residue (Methods) in solution (Figure 2a). Long single-molecule movies (30−40 min) were taken so that we could obtain enough binding and dissociation events (12−16 events on average) for each IgG molecule to calculate single-molecule kinetic constants. k_{on} and k_{off} were determined from intensity−time trajectories as the reciprocals of the average dwell times of the unbound and bound states, respectively, after removing artifacts based on localization information (Figure 2e and raw trajectories in Figure S3). The left panel of Figure 2b shows the scatter plot of the k_{on} and k_{off} values with each point representing an individual IgG molecule. The mean k_{on}, k_{off}, and K_D values were 0.73 ± 0.34 μM^{-1} s^{-1}, 0.62 ± 0.29 s^{-1}, and 0.94 ± 0.45 μM, respectively. Previously measured k_{on}, k_{off}, and K_D values ranged from 0.14 to 0.29 μM^{-1} s^{-1}, from 0.027 to 0.76 s^{-1}, and from 0.091 to 5.3 μM, respectively.[14−17] All previous studies used Fc fragments of IgG molecules from various sources and clones, and their measurements were performed in ensemble except for those of ref 13. In general, our results are in the same range as those previously measured. The surface density of IgG molecules was 0.75 μm^{-2}, as determined by the number of detected clusters per imaging area (Figure 2b, right).

A histogram of the fluorescence intensity of single complexes ($N = 198$) showed a single peak when localization information was used in analysis (Figure 2c, top), suggesting that pGB1 and IgG predominantly formed 1:1 complexes at 10 nM pGB1. The wide distribution of intensity is likely due to the nonuniformity in the illumination pattern. In contrast, an additional low-

DOI: 10.1021/acs.biochem.7b01293
Biochemistry 2018, 57, 1572−1576

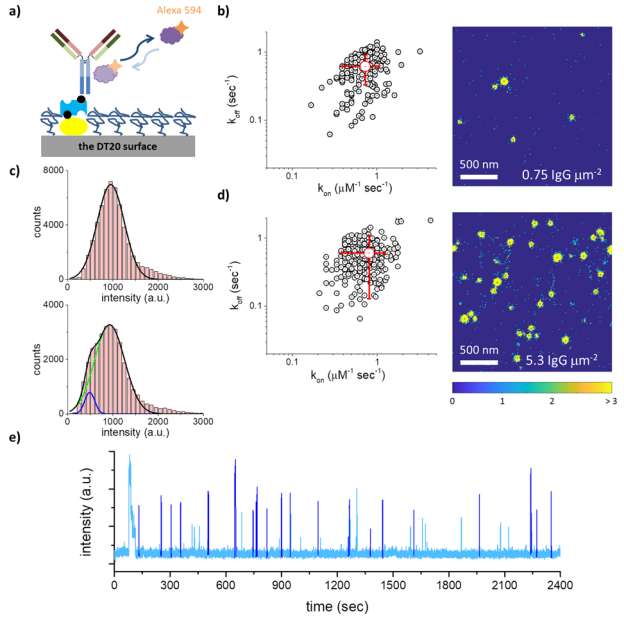

Figure 2. Binding assays for the pGB1−IgG interaction. (a) Schematics of measuring the pGB1−IgG interaction. (b) Scatter plot of the k_{on} and k_{off} values for each measured IgG molecule [N = 198 (left)]. The mean and standard deviation of the k_{on} and k_{off} values are indicated by the red label and error bars, respectively. A representative density map of localization events shows the positions of detected IgG molecules (right). The surface density of IgG molecules was 0.75 μm^{-2}. (c) Fluorescence intensity histograms of pGB1-bound states, obtained with (top) and without (bottom) localization information at 0.75 IgG μm^{-2}. (d) Same as panel b except that the surface density of IgG molecules was increased to 5.3 μm^{-2} and N = 272. The color bar in panels b and d indicates the number of localization events at each bin of the density maps (13 nm × 13 nm) (e) A representative intensity−time trajectory of the pGB1−IgG interaction at 5.3 IgG μm^{-2}. Using the method described for panels e and f of Figure 1 and Figure S2, intensity peaks were assigned to clusters. Intensity peaks colored dark blue belonged to the same IgG molecule. Other intensity peaks (light blue) belonged to either nonspecific binding events or closely spaced IgG molecules.

intensity peak showed up in the histogram obtained without localization information (Figure 2c, bottom). This second peak is likely due to binding events occurring slightly away from the receptors where the Gaussian kernel was centered, and those binding events were excluded from analysis when localization information was used. Because these two intensity peaks are largely overlapping, it is practically difficult to separate them through simple intensity thresholding, which emphasizes the necessity of using the single-molecule centroid localization algorithm to distinguish spatially close binding events. To estimate the contribution of the photobleaching rate to the estimated value of k_{off}, we doubly labeled pGB1 with Alexa 594 and biotin and directly immobilized it through a biotin−neutravidin linker. The photobleaching rate was negligible (0.005 s^{-1}) compared to the k_{off} value measured above (Figure S4).

We observed a relatively large variation in the measured k_{on} and k_{off} values among individual IgG molecules (Figure 2b). Because we collected only a finite number of dwell times for each IgG molecule (on average 12−16), we sought to determine how much variation is due to statistical uncertainty coming from finite sampling. We performed Gillespie simulation of the stochastic process of ligand binding and dissociation, with the experimental trajectory length and average rate constants as simulation parameters. The k_{on} and k_{off} values determined from the simulation had the same mean values as the experimental ones but a smaller standard deviation compared to that of the experimental ones (Figure S5), suggesting that additional heterogeneity among surface-immobilized IgG molecules is required to explain the observed variation.

We then increased the surface density of IgG molecules from 0.75 to 5.3 μm^{-2} so that a diffraction-limited minimal detection area would likely contain multiple IgG molecules. The kinetic and equilibrium constants measured at the high IgG density agreed well with those measured at the low density [k_{on} = 0.80 ± 0.42 μM^{-1} s^{-1}, k_{off} = 0.60 ± 0.47 s^{-1}, and K_D = 0.83 ± 0.48 μM (Figure 2d,e and raw trajectories in Figure S6)], demonstrating the effectiveness of our method in resolving closely spaced receptors. In comparison, when the same single-molecule movies were analyzed without localization information, the measured k_{on} values increased to 1.1 ± 0.75 and 2.8 ± 1.3 μM^{-1} s^{-1} for the cases of low and high IgG densities, respectively, and the measured K_D values decreased to 0.71 ± 0.46 and 0.20 ± 0.22 μM, respectively. The measured k_{off} values remained similar between two analyses (Figure S7). Using localization information as our "ground truth", we estimated the contribution of each type of artifact to these falsely high k_{on} values. At 0.75 IgG μm^{-2}, 67% of the trajectories analyzed without localization information were "contaminated" by nonspecific binding events (Figure 1d) and 34% contained multiple (on average 2.5) IgG molecules under a diffraction-limited minimal detection area (Figure 1e). At 5.3 IgG μm^{-2}, 80% of the trajectories were "contaminated" by nonspecific binding events and 97% contained multiple (on average 3.4) IgG molecules. Further analysis of nonspecific binding events on the imaging surface without immobilized IgG molecules yielded a $\Psi_{on,ns}$ value of 0.16 μm^{-2} μM^{-1} s^{-1} ($k_{on,ns} = A\Psi_{on,ns} \approx$ 0.06 μM^{-1} s^{-1}) and revealed that these events can be either transient or long-lived with the overall $k_{off,ns}$ value of 0.21 s^{-1} (Figure S1). Overall, ∼10% of all events were due to nonspecific binding when trajectories were analyzed without localization information. In addition, specific and nonspecific binding events had similar dissociation rate constants, partly explaining why k_{off} was not grossly miscalculated by conventional analysis.

Because the single-molecule centroid localization algorithm requires a certain level of image sparsity, ineffective surface passivation could affect the performance of centroid localization by attracting a large amount of long-lived nonspecifically bound ligands. Therefore, our method requires the use of reasonably well passivated imaging surfaces. For the same reason, the image sparsity condition also limits the surface density of receptors.[9] With 0.75 IgG μm^{-2} on the surface and 10 nM pGB1 in solution, we found the image sparsity condition was satisfied; with 5.3 IgG μm^{-2} on the surface, we could observe, in some frames, inaccurate centroid localization due to partially overlapping point spread functions (PSFs) where the surface density of receptors was high (data not shown). Because inaccurate centroid localization could affect the peak calling in our method, these regions were excluded from the analysis (Figure S8). The accuracy of centroid localization in high-density regions can be potentially improved by employing a more advanced centroid localization algorithm that was designed to localize partially overlapping PSFs.[19−21]

DOI: 10.1021/acs.biochem.7b01293
Biochemistry 2018, 57, 1572−1576

Next, we tested the versatility of our method by measuring the interaction between double-stranded DNA (dsDNA) and the Cas9−RNA complex. The Cas9−RNA complex consists of the endonuclease Cas9 and a guide RNA (gRNA). Cas9−RNA complex binding requires a protospacer-adjacent motif (PAM) on the target strand of dsDNA, and the k_{off} of this interaction depends on the length of matched sequences between gRNA and DNA adjacent to PAM. When there is only a short match (<9 bp) adjacent to PAM, Cas9−RNA complex binding is transient.[22] We used a DNA that has 4 bp PAM-proximal matches and 16 bp mismatches relative to the gRNA and a catalytically inactive mutant of Cas9.[22] The gRNA was biotinylated and immobilized on a PEG imaging surface through a biotin−neutravidin linker, while the DNA labeled with Cy3 was added in solution (Figure 3a). The kinetic and

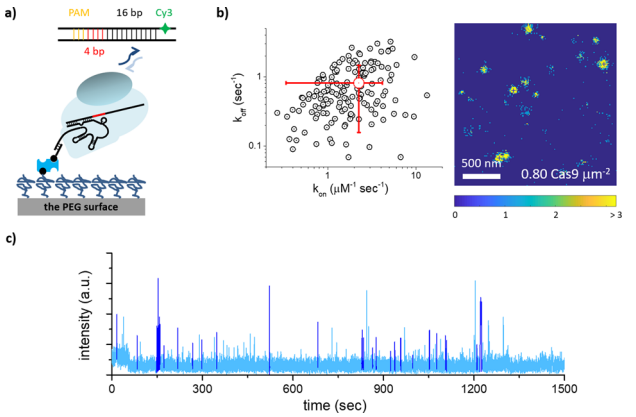

Figure 3. Binding assays for the interaction between dsDNA and the Cas9−RNA complex. (a) Schematics of measuring the interaction between dsDNA and the Cas9−RNA complex. The PAM motif (yellow) is adjacent to a 4 bp match (red) and then a 16 bp mismatch (black) region to the gRNA. (b) Scatter plot of the k_{on} and k_{off} values for each measured Cas9−RNA complex [N = 151 (left)]. The mean and standard deviation of the k_{on} and k_{off} values are indicated by the red label and error bars, respectively. A representative density map of localization events shows the positions of detected Cas9−RNA complexes (right). The surface density of Cas9−RNA complexes was 0.80 μm^{-2}. The color bar in panel b indicates the number of localization events at each bin of the density map (13 nm × 13 nm). (c) A representative intensity−time trajectory of the interaction between dsDNA and the Cas9−RNA complex. Using the method described for panels e and f of Figure 1 and Figure S2, intensity peaks were assigned to clusters. Intensity peaks colored dark blue belonged to the same Cas9−RNA complex. Other intensity peaks (light blue) belonged to either nonspecific binding events or closely spaced Cas9−RNA complexes.

equilibrium constants were determined with the same method described above, and the measured k_{on}, k_{off}, and K_D values were 2.3 ± 1.9 μM^{-1} s^{-1}, 0.82 ± 0.66 s^{-1}, and 0.48 ± 0.34 μM, respectively (Figure 3b,c and raw trajectories in Figure S9), in agreement with those previously measured by single-molecule FRET between a Cy3 (donor)-labeled DNA immobilized on the surface and a Cy5 (acceptor)-labeled Cas9−RNA complex in solution (k_{on} = 4−8 μM^{-1} s^{-1}, and k_{off} = 0.8−4 s^{-1}).[22] In comparison, when the same single-molecule movies were analyzed without localization information, the measured k_{on}, k_{off}, and K_D values became 2.4 ± 1.5 μM^{-1} s^{-1}, 0.91 ± 0.71 s^{-1}, and 0.42 ± 0.26 μM, respectively. We did not observe an improvement using localization information likely because the receptor density was not high, and the PEG surface was effective in preventing the nonspecific binding of DNA.

In summary, we demonstrated that the accuracy of fluorescence binding assays can be improved by using the single-molecule centroid localization algorithm. The two major artifacts in this type of assay, i.e., nonspecific binding events and optically overlapping receptors, can be detected and corrected during analysis. For instance, apparent binding rate constant $k_{on,app}$ of the pGB1−IgG interaction on the DT20 surface is equal to $n \times 0.73\ \mu M^{-1}\ s^{-1} + A \times 0.16\ \mu m^{-2}\ \mu M^{-1}\ s^{-1}$. With localization information, n is equal to 1. Also, because the minimal detection area is reduced after data acquisition through the single-molecule centroid localization algorithm, the $A\Psi_{on,ns}$ term is reduced at least 100 times compared to that of conventional analysis (and this is considering a moderate 10 times higher lateral resolution in the x and y directions). Besides, having high densities of receptors allows us to obtain the same amount of data with relatively small EMCCD regions. Therefore, we can image at a higher time resolution with a higher efficiency. This analysis routine requires little modification to common experimental protocols and could be performed synergistically with existing methods (e.g., multi-color co-localization analysis), making it readily applicable to existing data and future experiments.

■ ASSOCIATED CONTENT

Supporting Information

The Supporting Information is available free of charge on the ACS Publications website at DOI: 10.1021/acs.biochem.7b01293.

Experimental details and supplementary figures (PDF)

Movie 1 (AVI)

■ AUTHOR INFORMATION

Corresponding Author

*E-mail: tjha@jhu.edu.

ORCID

Boyang Hua: 0000-0002-8869-9762

Kyu Young Han: 0000-0002-1448-3125

Wei Cheng: 0000-0003-0332-1566

Present Addresses

#S.P.: Department of Biochemistry and Molecular Biology, The University of Chicago, Chicago, IL 60637.

@K.Y.H.: CREOL, the College of Optics and Photonics, University of Central Florida, Orlando, FL 32816.

∇J.H.K.: Department of Microbiology & Immunology, College of Medicine, University of South Alabama, Mobile, AL 36688.

Author Contributions

B.H., W.C., and T.H. designed the project. B.H., Y.W., D.S., and J.H.K. performed the experiments. D.S. provided the Cy3-labeled dsDNA and biotinylated Cas9−RNA complex samples. J.H.K. provided the Alexa 594-labeled protein G B1 domain sample. B.H., S.P., and K.Y.H. wrote the data analysis software and analyzed the data. B.H., W.C., and T.H. wrote the manuscript.

Funding

This work was supported by grants from the National Institutes of Health (R35 GM122569 to T.H. and DP2 OD008693 to W.C.) and the National Science Foundation (PHY 1430124 to T.H. and CHE 1149670 to W.C.) and the Upjohn Research

DOI: 10.1021/acs.biochem.7b01293
Biochemistry 2018, 57, 1572−1576

Award to W.C. T.H. is an investigator of the Howard Hughes Medical Institute.

Notes

The authors declare no competing financial interest.

REFERENCES

(1) Pollard, T. D. (2010) A guide to simple and informative binding assays. *Mol. Biol. Cell 21*, 4061−4067.
(2) Elenko, M. P., Szostak, J. W., and van Oijen, A. M. (2009) Single-Molecule Imaging of an in Vitro-Evolved RNA Aptamer Reveals Homogeneous Ligand Binding Kinetics. *J. Am. Chem. Soc. 131*, 9866−9867.
(3) Jungmann, R., Steinhauer, C., Scheible, M., Kuzyk, A., Tinnefeld, P., and Simmel, F. C. (2010) Single-Molecule Kinetics and Super-Resolution Microscopy by Fluorescence Imaging of Transient Binding on DNA Origami. *Nano Lett. 10*, 4756−4761.
(4) Friedman, L. J., Chung, J., and Gelles, J. (2006) Viewing dynamic assembly of molecular complexes by multi-wavelength single-molecule fluorescence. *Biophys. J. 91*, 1023−1031.
(5) Hua, B., Han, K. Y., Zhou, R., Kim, H., Shi, X., Abeysirigunawardena, S. C., Jain, A., Singh, D., Aggarwal, V., Woodson, S. A., and Ha, T. (2014) An improved surface passivation method for single-molecule studies. *Nat. Methods 11*, 1233−1236.
(6) Levene, M. J., Korlach, J., Turner, S. W., Foquet, M., Craighead, H. G., and Webb, W. W. (2003) Zero-mode waveguides for single-molecule analysis at high concentrations. *Science 299*, 682−686.
(7) Acuna, G. P., Möller, F. M., Holzmeister, P., Beater, S., Lalkens, B., and Tinnefeld, P. (2012) Fluorescence enhancement at docking sites of DNA-directed self-assembled nanoantennas. *Science 338*, 506−510.
(8) Sharonov, A., and Hochstrasser, R. M. (2006) Wide-field subdiffraction imaging by accumulated binding of diffusing probes. *Proc. Natl. Acad. Sci. U. S. A. 103*, 18911−18916.
(9) Jungmann, R., Avendaño, M. S., Dai, M., Woehrstein, J. B., Agasti, S. S., Feiger, Z., Rodal, A., and Yin, P. (2016) Quantitative super-resolution imaging with qPAINT. *Nat. Methods 13*, 439−442.
(10) Johnson-Buck, A., Nangreave, J., Kim, D. N., Bathe, M., Yan, H., and Walter, N. G. (2013) Super-Resolution Fingerprinting Detects Chemical Reactions and Idiosyncrasies of Single DNA Pegboards. *Nano Lett. 13*, 728−733.
(11) Akerström, B., Nielsen, E., and Björck, L. (1987) Definition of IgG- and albumin-binding regions of streptococcal protein G. *J. Biol. Chem. 262*, 13388−13391.
(12) Akerström, B., and Björck, L. (1986) A physicochemical study of protein G, a molecule with unique immunoglobulin G-binding properties. *J. Biol. Chem. 261*, 10240−10247.
(13) Sjöbring, U., Björck, L., and Kastern, W. (1991) Streptococcal protein G. Gene structure and protein binding properties. *J. Biol. Chem. 266*, 399−405.
(14) Cao, Y., Balamurali, M. M., Sharma, D., and Li, H. (2007) A functional single-molecule binding assay via force spectroscopy. *Proc. Natl. Acad. Sci. U. S. A. 104*, 15677−15681.
(15) Powell, K. D., Ghaemmaghami, S., Wang, M. Z., Ma, L., Oas, T. G., and Fitzgerald, M. C. (2002) A General Mass Spectrometry-Based Assay for the Quantitation of Protein−Ligand Binding Interactions in Solution. *J. Am. Chem. Soc. 124*, 10256−10257.
(16) Gülich, S., Linhult, M., Ståhl, S., and Hober, S. (2002) Engineering streptococcal protein G for increased alkaline stability. *Protein Eng., Des. Sel. 15*, 835−842.
(17) Walker, K. N., Bottomley, S. P., Popplewell, A. G., Sutton, B. J., and Gore, M. G. (1995) Equilibrium and pre-equilibrium fluorescence spectroscopic studies of the binding of a single-immunoglobulin-binding domain derived from protein G to the Fc fragment from human IgG1. *Biochem. J. 310*, 177−184.
(18) van Oijen, A. M. (2011) Single-molecule approaches to characterizing kinetics of biomolecular interactions. *Curr. Opin. Biotechnol. 22*, 75−80.
(19) Holden, S. J., Uphoff, S., and Kapanidis, A. N. (2011) DAOSTORM: an algorithm for high- density super-resolution microscopy. *Nat. Methods 8*, 279−280.
(20) Huang, F., Schwartz, S. L., Byars, J. M., and Lidke, K. A. (2011) Simultaneous multiple-emitter fitting for single molecule super-resolution imaging. *Biomed. Opt. Express 2*, 1377−1393.
(21) Cox, S., Rosten, E., Monypenny, J., Jovanovic-Talisman, T., Burnette, D. T., Lippincott-Schwartz, J., Jones, G. E., and Heintzmann, R. (2012) Bayesian localization microscopy reveals nanoscale podosome dynamics. *Nat. Methods 9*, 195−200.
(22) Singh, D., Sternberg, S. H., Fei, J., Doudna, J. A., and Ha, T. (2016) Real-time observation of DNA recognition and rejection by the RNA-guided endonuclease Cas9. *Nat. Commun. 7*, 12778.

DOI: 10.1021/acs.biochem.7b01293
Biochemistry 2018, 57, 1572−1576